Effective shell-model interaction for nuclei "southeast" of ^{100}Sn

Z. H. Sun [1,2] G. Hagen [2,1] G. R. Jansen [3,2] and T. Papenbrock [1,2]

[1]*Department of Physics and Astronomy, University of Tennessee, Knoxville, Tennessee 37996, USA*

[2]*Physics Division, Oak Ridge National Laboratory, Oak Ridge, Tennessee 37831, USA*

[3]*National Center for Computational Sciences, Oak Ridge National Laboratory, Oak Ridge, Tennessee 37831, USA*

(Received 29 July 2021; accepted 1 December 2021; published 14 December 2021)

We construct an effective shell-model interaction for the valence space spanned by single-particle neutron and single-hole proton states in ^{100}Sn. Starting from chiral nucleon-nucleon and three-nucleon forces and single-reference coupled-cluster theory for ^{100}Sn we apply a second similarity transformation that decouples the valence space. The particle-particle components of the resulting effective interaction can be used in shell model calculations for neutron deficient tin isotopes. The hole-hole interaction can be used to calculate the $N = 50$ isotones south of ^{100}Sn, and the full particle-hole interaction describes nuclei in the region southeast of ^{100}Sn. We compute low-lying excited states in selected nuclei southeast of ^{100}Sn, and find reasonable agreement with data. The presented techniques can also be applied to construct effective shell-model interactions for other regions of the nuclear chart.

DOI: 10.1103/PhysRevC.104.064310

I. INTRODUCTION

The shell model is the paradigm to understand the structure of atomic nuclei and to compute their properties [1–4]. In this model, valence nucleons move within the mean field produced by the inert core and interact via a residual effective interaction. For a recent review of the long and winding road to effective shell-model interactions, we refer the reader to Ref. [5] and briefly summarize some developments in what follows. For a given model space, the matrix elements of the effective interaction are often determined phenomenologically by fit to data [6–8], or by tweaking the monopole terms [9] of a microscopically derived G matrix [10]. More microscopic approaches [11,12] are based on many-body perturbation theory which, however, poses its own challenges [13,14] and requires resummations [15,16]. Recent extensions of such approaches Coraggio *et al.* [17] sum up the irreducible two-body diagrams to infinite order and subtract the one-body components. The starting point typically are low-momentum nucleon-nucleon potentials [18] with a suitably chosen cutoff [19,20].

Effective interactions can also be derived without tuning any adjustable parameters when starting from nucleon-nucleon and three-nucleon potentials [21–27]. Several of these approaches require one to decouple the two-body interaction in a small shell-model space from the (infinite) Hilbert space. Here, similarity transformations play a key role. These can be based on the Lee-Suzuki approaches [28,29], coupled-cluster theory [22,30,31], or the in-medium similarity renormalization group (IMSRG) [32–34].

In this paper, we develop an effective shell-model interaction for nuclei southeast of ^{100}Sn based on similarity transformations. This region of the nuclear chart is interesting because its cornerstone—the doubly magic $N = Z = 50$ nucleus ^{100}Sn—is close to the proton dripline, the endpoint of α decays [35,36], and exhibits one of the strongest Gamow-Teller matrix elements [37–39]. Several recent experiments studied the structure of nuclei in this part of the nuclear chart [40–44]. Traditionally, shell-model computations of nuclei in this region start from a ^{88}Sr or ^{90}Zr core [45,46]. In such an approach, the proton shell is almost full once elements close to tin have been reached, in addition, the computational cost quickly becomes a bottleneck (see, e.g., [46]), which makes it attractive to compute a particle-hole shell-model interaction starting from ^{100}Sn. We note that ^{100}Sn can be computed from scratch using coupled-cluster theory [46], and this nucleus is predicted to be a "better," i.e., more strongly bound, core than ^{88}Sr [45].

Recent nonperturbative approaches to effective interactions include methods that are based on many-body wave functions calculated with *ab-initio* methods such as no-core shell model (NCSM) [25,47] and coupled-cluster theory [22,23]. Once the wave functions of $A_{\rm core} + 1$ and $A_{\rm core} + 2$ are obtained, the effective interaction can be extracted through a Lee-Suzuki transformation [28,29,48,49]. Effective interactions derived through these approaches decouple the model space from the excluded space on the two- and three-body levels without introducing additional parameters. In principle, these nonperturbative methods also work for multishell spaces. However, it is challenging to obtain converged full-space wave functions for all allowed quantum numbers defined by the valence space, and for heavy nuclei. In the coupled-cluster implementation, for instance, some observables are sensitive to small contributions from high-lying excited states.

This computational problem is, to some extent, overcome by the valence-space IMSRG (VS-IMSRG) [34,50,51], and

the shell-model coupled-cluster (SMCC) [26] approaches. Instead of employing the A-body wave functions in Hilbert space, VS-IMSRG and SMCC are straightforward extensions of IMSRG and coupled-cluster theory, respectively, to open-shell nuclei. Similarity transformations are applied to the normal-ordered Hamiltonian to decouple the model space and these approaches are suitable to calculate medium-heavy nuclei. Recently the VS-IMSRG was successfully applied to compute nuclei in the island of inversion region by decoupling a multishell valence space [52].

In this paper we select the core nearest to the target nuclei and perform a shell model calculation with both particles and holes. The effective interaction is derived through the particle-hole shell-model coupled-cluster approach (*ph*-SMCC). In *ph*-SMCC we treat the three-body correlations in a single-reference coupled-cluster approach instead of in the shell-model effective interaction. This is an advantage because the coupled-cluster method is more accurate than SMCC in dealing with the induced three-body correlations. The ph-SMCC is an extension of SMCC, in which a secondary similarity transformation is applied to the coupled-cluster effective Hamiltonian. The resulting Hamiltonian decouples the excluded space and the valence space, and the latter is spanned by particle and hole states. Once the Hamiltonian is decoupled, the valence effective interaction consists of particle-particle (*pp*), hole-hole (*hh*), and particle-hole (*ph*) channels. The *pp* channel is a conventional shell model effective interaction, and particle-removed nuclei can be calculated with the *hh* interaction. The *ph* channel can be used to calculate nuclei located in the southeast and northwest of a double magic nucleus, i.e., as protons removed, and neutrons attached, or vice versa. The particle-hole decoupling is equivalent to a conventional decoupling with the core in the valence space, and this is similar to the ensemble normal-ordering used in the VS-IMSRG [51]. The resulted effective particle-hole interaction can be re-normal-ordered with respect to a smaller core to obtain a more conventional *pp* interaction.

The paper is organized as follows. In Sec. II, we briefly introduce the single-reference coupled-cluster method and the resulting similarity-transformed Hamiltonian. This is followed by the derivation of the particle-hole decoupling. In Sec. III we apply the *ph*-SMCC method to the ^{100}Sn region using two different chiral nucleon-nucleon and three-nucleon potentials. Finally, we summarize our results.

II. SHELL-MODEL COUPLED-CLUSTER PARTICLE AND HOLE INTERACTION

A. Shell-model coupled cluster

The coupled-cluster method [30,31,53–56] is useful for *ab-initio* calculations of medium-mass nuclei [46,57]. Our coupled-cluster calculations start from the intrinsic Hamiltonian,

$$H = \left(1 - \frac{1}{A}\right) \sum_{i=1}^{A} \frac{p_i^2}{2m} + \sum_{i<j=1}^{A} \left(v_{ij} - \frac{\vec{p_i}\,\vec{p_j}}{mA}\right) + \sum_{i<j<k}^{A} v_{ijk}. \tag{1}$$

Here, m is the mass of the nucleon, p_i and p_j are the single-particle momentum, A is the mass number, v_{ij} is the nucleon-nucleon potential, and v_{ijk} is the three-body potential defined in the laboratory coordinates. The Hamiltonian is henceforth normal-ordered with respect to a reference state $|\Phi_0\rangle$, e.g., a Hartree-Fock (HF) state or a product state of natural orbitals. We denote the energy expectation value of the reference state as $E_0 = \langle\Phi_0|H|\Phi_0\rangle$. The normal-ordered Hamiltonian is

$$\mathcal{H} = E_0 + \sum_{pq} f_{pq}\{p^\dagger q\} + \frac{1}{4}\sum_{pqrs} V_{pqrs}\{p^\dagger q^\dagger sr\} \tag{2}$$

$$+ \frac{1}{36}\sum_{pqrstu} V_{pqr,stu}\{p^\dagger q^\dagger r^\dagger stu\}. \tag{3}$$

Here, we use $p^\dagger$ as the particle or hole creation operator on state $|\phi_p\rangle$, and p is the annihilation operator. The one-body Fock matrix has elements f_{pq}, while V_{pqrs} and $V_{pqr,stu}$ denote the two-body and three-body matrix elements, respectively. To avoid dealing with the three-body diagrams after normal-ordering, Eq. (2) is usually truncated at the two-body level and the residual three-body terms are discarded. This approximation is accurate in ^{4}He [58], ^{16}O [59], and nuclear matter [60] (albeit only for three-nucleon forces with nonlocal regulators).

Coupled cluster theory is based on the exponential ansatz

$$|\Phi\rangle = e^T|\Phi_0\rangle, \tag{4}$$

where T is the cluster operator

$$T = T_1 + T_2 + T_3 + \cdots, \tag{5}$$

that introduces one-particle–one-hole ($1p$–$1h$), $2p$–$2h$, $3p$–$3h$,...,Ap–Ah excitations. The np–nh excitation operator is

$$T_n = \frac{1}{(n!)^2}\sum_{\substack{i_1,i_2,\ldots,i_n\\ a_1,a_2,\ldots,a_n}} t^{a_1,a_2,\ldots,a_n}_{i_1,i_2,\ldots,i_n}\{a_1^\dagger a_2^\dagger\cdots a_n^\dagger i_1 i_2\cdots i_n\}. \tag{6}$$

The Schrödinger equation is then written as

$$\mathcal{H}e^T|\Phi_0\rangle = Ee^T|\Phi_0\rangle. \tag{7}$$

Left multiplication with e^{-T} on both sides of Eq. (7) yields

$$e^{-T}\mathcal{H}e^T|\Phi_0\rangle = E|\Phi_0\rangle. \tag{8}$$

Equation (8) indicates that the reference state $|\Phi_0\rangle$ is an eigenstate of the similarity-transformed Hamiltonian

$$\overline{\mathcal{H}} \equiv e^{-T}\mathcal{H}e^T. \tag{9}$$

In other words, $\overline{\mathcal{H}}$ generates no *ph* excitations of the reference, and

$$\langle\Phi^{a_1a_2\cdots a_n}_{i_1i_2\cdots i_n}|\overline{\mathcal{H}}|\Phi_0\rangle = 0. \tag{10}$$

The T amplitudes fulfill Eq. (10) and thereby decouple the reference state from all excited states. The similarity transformed Hamiltonian can be expanded as

$$\overline{\mathcal{H}} = E_{CC} + \sum_{pq}\overline{\mathcal{H}}_{pq}\{p^\dagger q\} + \sum_{pqrs}\overline{\mathcal{H}}_{pqrs}\{p^\dagger q^\dagger sr\}$$

$$+ \sum_{pqrstu}\overline{\mathcal{H}}_{pqrstu}\{p^\dagger q^\dagger r^\dagger uts\} + \cdots, \tag{11}$$

and contains—when T is not truncated—A-body operators, even when the normal-ordered Hamiltonian $\mathcal{H}$ has lower rank. Here, $E_{CC} = \langle\Phi_0|\overline{\mathcal{H}}|\Phi_0\rangle$ is the correlation energy. In practice, the cluster operator in Eq. (5) is truncated to avoid the exponential computational expense of full configuration mixing. Truncation to $T = T_1 + T_2$ yields the coupled-cluster singles and doubles (CCSD) approximation.

Single-reference coupled-cluster theory is most efficient to calculate closed-shell nuclei. Open-shell systems can be computed by starting from a deformed, symmetry-breaking reference state [61], and the broken symmetry needs to be restored through angular momentum projection [62,63]. Another approach to open-shell nuclei employs equation-of-motion methods (EOM-CC) [23,64–66]; these are restricted to neighbors of closed-shell nuclei

The SMCC method is an alternative approach to treat the open-shell problem with coupled-cluster methods by creating an effective interaction to be used in shell-model calculations. In such a calculation, the effective interaction is defined in a model space spanned by one or two major shells, whereas $\overline{\mathcal{H}}$ is defined in the full space defined by several shells in the harmonic-oscillator basis. To construct a shell-model effective interaction, the Hilbert space is split into the model space P, and its complement Q, where

$$P + Q = \mathbf{1}. \tag{12}$$

The task is then to decouple the P space from the Q space for the Hamiltonian. To accomplish this, a secondary similarity transformation is applied to the coupled-cluster Hamiltonian,

$$\overline{\overline{\mathcal{H}}} = e^{-S}\overline{\mathcal{H}}e^{S}, \tag{13}$$

and the decoupling between P and Q space requires

$$Q\overline{\overline{\mathcal{H}}}P = 0. \tag{14}$$

Equation (14) is an A-body equation and S is also an A-body operator. In what follows, we use S_{pp} to represent the S operator in particle-particle decoupling, S_{hh} for that in the hole-hole decoupling, S_{hp} for particle and hole decoupling, and S with no subscript for any combination of them. On the two-body level, S_{pp} has the form

$$S_{pp} = \sum_{av_1} s^{a}_{v_1}\{a^\dagger v_1\} + \sum_{abv_1v_2} s^{ab}_{v_1v_2}\{a^\dagger b^\dagger v_1 v_2\} + \sum_{abhv} s^{ab}_{hv}\{a^\dagger b^\dagger hv\} + \cdots . \tag{15}$$

Here, we used v to represent valence state, while $a, b, c, \ldots$ and $i, j, k, \ldots$ denote particle and hole states, respectively. The first term in Eq. (15) represents a valence particle v_1 coupled to a state outside the model space a through a one-body operator [see diagram (a) in Fig. 1], the second term couples two particles inside the model space to a state which has at least one particle outside the model space [see diagram (b) in Fig. 1], and the third term couples the valence state to particle-hole configurations [see diagram (c) in Fig. 1]. One can write down three-body terms (and operators of higher rank) in a similar manner.

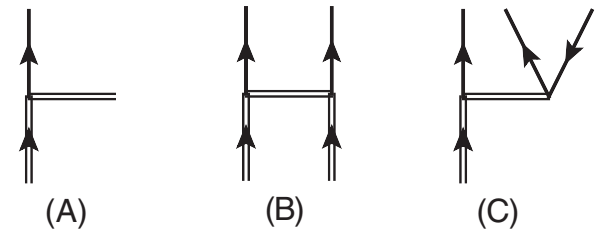

FIG. 1. Diagrammatic representation of the decoupling generator S_{pp}. The horizontal line is the S_{pp} operator, with the particles indicated by incoming and outgoing arrow lines. The model-space particles indicated by incoming double lines

In this paper, we truncate Eqs. (14) and (15) at the two-body level and refer to this as the SMCC(2) approximation. The two-body level decoupling condition (14) becomes

$$\langle a|\overline{\overline{\mathcal{H}}}|v_1\rangle = 0, \tag{16}$$

$$\langle ab|\overline{\overline{\mathcal{H}}}|v_1v_2\rangle = 0, \tag{17}$$

$$\langle ab|\overline{\overline{\mathcal{H}}}|iv_1\rangle = 0. \tag{18}$$

Once decoupled, the effective Hamiltonian is

$$H_{\text{eff}} = P\overline{\overline{\mathcal{H}}}P, \tag{19}$$

which is defined only inside the model space. In principle, the Hamiltonian H_{eff} reproduces a subset of the eigenvalues of $\overline{\mathcal{H}}$. In practice, however, the truncation of many-body terms leads to a discrepancy of eigenvalues between H_{eff} and $\overline{\overline{\mathcal{H}}}$, because the truncation of many-body terms breaks the similarity of the transformation. The quality of the effective interaction thus depends on whether the neglected many-body terms are small compared to the retained two-body matrix elements [26].

The evaluation of $\overline{\overline{\mathcal{H}}}$ via Eq. (13) is nontrivial due to the properties of S. In single-reference coupled-cluster theory, the operator T only consists of excitation operators, and we have

$$[T_m, T_n] = 0, \tag{20}$$

i.e., different excitations commute. Thus, H can only contract with T from the right side, and Eq. (8) terminates exactly on the fourth nested commutator in CCSD for two-body Hamiltonians. In contrast, the operator S in SMCC consists of both excitation and de-excitation operators, and these do not commute with each other, i.e.,

$$[S_m, S_n] \neq 0. \tag{21}$$

Consequently, $\overline{\mathcal{H}}$ can contract with S from both the left and the right side and the evaluation of $\overline{\overline{\mathcal{H}}}$ does not terminate within the Baker-Campbell–Hausdorff (BCH) expansion,

$$\overline{\overline{\mathcal{H}}} = \overline{\mathcal{H}} + [\overline{\mathcal{H}}, S] + \frac{1}{2!}[[\overline{\mathcal{H}}, S], S] + \cdots . \tag{22}$$

Equation (22) is a set of nonlinear coupled equations, meanwhile, the nonterminating BCH expansion complicates the evaluation of $\overline{\overline{\mathcal{H}}}$. We note that a truncation of Eq. (22) is not accurate. In this present work we adopt an approach that is similar to the Magnus method [67] from the IMSRG [68]. The

idea is to make S dependent on a flow parameter t and then to replace Eq. (13) by the differential equation

$$\frac{\partial \overline{\overline{\mathcal{H}}}(t)}{\partial t} = \left[\overline{\overline{\mathcal{H}}}(t), \frac{\partial S}{\partial t}\right]. \tag{23}$$

Using the initial condition $\overline{\overline{\mathcal{H}}}(0) = \overline{\mathcal{H}}$ and choosing $S(0)$ as the off-diagonal part of $\overline{\overline{\mathcal{H}}}$ then requires us to numerically integrate Eq. (23). We obtain the operators $S(t)$ and $\overline{\overline{\mathcal{H}}}(t)$ as solutions, and the corresponding matrix elements become constant for sufficiently large values of the flow parameter t. When performing the integration, $\overline{\overline{\mathcal{H}}}$ develops more than two-body terms (even when $\overline{\mathcal{H}}$ is of two-body rank), because the commutator of two two-body operators is in general a three-body operator. The induced three-body force can link the valence space and the excluded space via an off-diagonal three-body term S_{3b}. The diagonal three-body terms also contribute to the BCH expansion through $[H_{3b}, S_{2b}]_{2b}$. The explicit evaluation of the three-body terms is challenging and numerically expensive [69]. We therefore follow the nonperturbative IMSRG(2) approximation of Ref. [34] and truncate each commutator at the two-body level. This approximation is motivated by the success of the coupled-cluster and IMSRG computations when contributions from three-body operators are truncated at the normal-ordered two-body level [34,58,59]. In the BCH expansion nested commutators are computed to very high order until they become numerically very small; this makes the expansion nonperturbative. The rank of operators kept in the expansion, however, is truncated at two, i.e., only normal-ordered two-body operators are kept. The solution of Eq. (23) thus becomes $\overline{\overline{\mathcal{H}}} = \overline{\overline{\mathcal{H}}}_{1b} + \overline{\overline{\mathcal{H}}}_{2b}$.

When solving Eq. (23) we compute nested commutators recursively via

$$D^{(n)} = [D^{(n-1)}, S]_{2b}. \tag{24}$$

Here, $D^{(0)} = \overline{\mathcal{H}}$. This allows us to rewrite Eq. (22) as

$$\overline{\overline{\mathcal{H}}} = \sum_{n=0} \frac{1}{n!} D^{(n)}. \tag{25}$$

Let us discuss the contribution of the neglected higher-body terms. To make estimates we turn to the BCH expansion (22) and assume that any corrections of S are small. (We note that S is dimensionless.) The leading contribution from three-body terms to two-body terms are $[[D, S_{2b}]_{3b}, S_{2b}]_{2b}$. Sun *et al.* [26] found that this commutator yielded a much smaller contribution to $\overline{\overline{\mathcal{H}}}$ than the leading term $[D, S_{3b}]_{2b}$ from the three-body operator S_{3b}. Thus, we approximate the leading induced three-body force as

$$\overline{\overline{\mathcal{H}}}_{3b} = [\overline{\mathcal{H}}_{2b}, S_{2b}]_{3b}. \tag{26}$$

We note that this approximation, while well motivated, is in the end a pragmatic choice. Below we gauge its accuracy by comparison to more precise computations.

The main task is then to calculate the contraction $[D^{(n)}, S]$. We find

$$\begin{aligned} D^{(n+1)}{}^{ia}_{bc} &= (1 - P_{bc})\left(\sum_e D^{(n)}{}^{ia}_{be} S^e_c + \sum_{je} D^{(n)}{}^{ij}_{be} S^{ea}_{jc}\right) \\ &\quad - \sum_e \left(D^{(n)}{}^{ie}_{bc} S^a_e - D^{(n)}{}^{i}_{e} S^{ea}_{bc}\right) \\ &\quad + \frac{1}{2}\sum_{ef} D^{(n)}{}^{ia}_{ef} S^{ef}_{bc}, \end{aligned} \tag{27}$$

$$D^{(n+1)}{}^{ij}_{ka} = \frac{1}{2}\sum_{ef} D^{(n)}{}^{ij}_{ef} S^{ef}_{ka} + \sum_e D^{(n)}{}^{ij}_{ke} S^e_a, \tag{28}$$

$$\begin{aligned} D^{(n+1)}{}^{ia}_{jb} &= \sum_e \left(D^{(n)}{}^{ia}_{je} S^e_b - D^{(n)}{}^{ie}_{jb} S^a_e + D^{(n)}{}^{i}_{e} S^{ea}_{jb}\right) \\ &\quad + \frac{1}{2}\sum_{ef} D^{(n)}{}^{ia}_{ef} S^{ef}_{jb} + \sum_{ke} D^{(n)}{}^{ik}_{je} S^{ea}_{kb}, \end{aligned} \tag{29}$$

$$\begin{aligned} D^{(n+1)}{}^{ab}_{cd} &= \frac{1}{2}\sum_{ef} \left(D^{(n)}{}^{ab}_{ef} S^{ef}_{cd} - S^{ab}_{ef} D^{(n)}{}^{ef}_{cd}\right) \\ &\quad + \sum_e (1 - P_{cd})\left(D^{(n)}{}^{ab}_{ce} S^e_d - S^{ab}_{ce} D^{(n)}{}^{e}_{d}\right) \\ &\quad - \sum_e (1 - P_{ab})\left(D^{(n)}{}^{eb}_{cd} S^a_e - S^{eb}_{cd} D^{(n)}{}^{a}_{e}\right) \\ &\quad - \sum_k (1 - P_{cd}) D^{(n)}{}^{k}_{c} S^{ab}_{kd} \\ &\quad + \sum_{je} (1 - P_{ab})(1 - P_{cd}) D^{(n)}{}^{ja}_{ec} S^{eb}_{jd}, \end{aligned} \tag{30}$$

$$D^{(n+1)}{}^{ij}_{kl} = 0, \tag{31}$$

and

$$\begin{aligned} D^{(n+1)}{}^{ab}_{ic} &= \frac{1}{2}\sum_{ef} \left(D^{(n)}{}^{ab}_{ef} S^{ef}_{ic} - S^{ab}_{ef} D^{(n)}{}^{ef}_{ic}\right) \\ &\quad + \sum_e \left(D^{(n)}{}^{ab}_{ie} S^e_c - D^{(n)}{}^{e}_{c} S^{ab}_{ie}\right) \\ &\quad + \sum_e (1 - P_{ab})\left(D^{(n)}{}^{b}_{e} S^{ae}_{ic} - S^{b}_{e} D^{(n)}{}^{ae}_{ic}\right) \\ &\quad - \sum_k S^{ab}_{kc} D^{(n)}{}^{k}_{i} - \sum_{je} (1 - P_{ab}) D^{(n)}{}^{ja}_{ie} S^{eb}_{jc}, \end{aligned} \tag{32}$$

$$D^{(n+1)}{}^{ia}_{jk} = -\sum_e D^{(n)}{}^{ie}_{jk} S^a_e, \tag{33}$$

$$D^{(n+1)}{}^{ij}_{ab} = \frac{1}{2}\sum_{ef} D^{(n)}{}^{ij}_{ef} S^{ef}_{ab} + \sum_e (1 - P_{ab}) D^{(n)}{}^{ij}_{ae} S^e_b. \tag{34}$$

We make an initial guess of the S operator, compute the operator $\overline{\overline{\mathcal{H}}}$ and update S accordingly. By repeating this procedure we integrate out the off-diagonal pieces of $\overline{\mathcal{H}}$ until the decoupling condition is fulfilled.

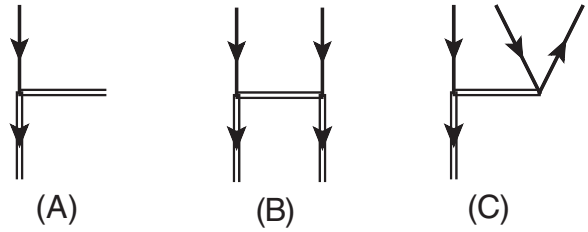

FIG. 2. Diagrammatic representation of S_{hh}. The horizontal line is the S_{hh} operator, with the particles and holes indicated by incoming and outgoing arrow lines. The model-space holes indicated by outgoing double lines

B. Particle-hole shell model coupled cluster

Before moving to the particle-hole decoupling, we derive the effective hole-hole interaction. A hole-hole decoupling yields an effective interaction for valence holes. On the two-body level, the operator S for hole-hole decoupling is

$$S_{hh} = \sum_{iv_1} s_i^{v_1}\{v_1^\dagger i\} + \sum_{v_1 v_2 ij} s_{ij}^{v_1 v_2}\{v_1^\dagger v_2^\dagger ij\} + \sum_{ijv_1 a} s_{ij}^{v_1 a}\{v_1^\dagger a^\dagger ij\}. \tag{35}$$

Here, v_i denotes a valence-hole state. The first two terms link valence holes and holes outside the model space through a one- and two-body operator, and the last term is the single hole coupled to the particle-hole excitation configurations. Diagrams representing Eq. (35) are shown in Fig. 2.

Similar to the particle-particle decoupling, S_{hh} is determined through solving the decoupling equation (14). The two-body level decoupling equation for the hole-hole effective interaction is

$$\langle v_1|\overline{\overline{\mathcal{H}}}|i\rangle = 0, \tag{36}$$

$$\langle v_1 v_2|\overline{\overline{\mathcal{H}}}|ij\rangle = 0, \tag{37}$$

$$\langle v_1 a|\overline{\overline{\mathcal{H}}}|ij\rangle = 0. \tag{38}$$

Once decoupled, the hole-hole sector of $\overline{\overline{\mathcal{H}}}$ should reproduce a subset of eigenvalues of particle removed systems.

Using the two-body level S for the hole-hole decoupling in Eq. (35), the single commutator yields

$$D^{(n+1)}{}^{ia}_{bc} = \frac{1}{2}\sum_{kl} D^{(n)}{}^{kl}_{bc} S^{ia}_{kl} - \sum_{k} D^{(n)}{}^{ka}_{bc} S^{i}_{k}, \tag{39}$$

$$\begin{aligned} D^{(n+1)}{}^{ij}_{ka} = &-\sum_{l}(1-P_{ij}) D^{(n)}{}^{lj}_{ka} S^{i}_{l} + \sum_{bl}(1-P_{ij}) D^{(n)}{}^{lj}_{ba} S^{ib}_{kl} \\ &+ \sum_{l}\left(D^{(n)}{}^{ij}_{la} S^{l}_{k} - S^{ij}_{kl} D^{(n)}{}^{l}_{a}\right) + \frac{1}{2}\sum_{lm} D^{(n)}{}^{lm}_{ka} S^{ij}_{lm}, \end{aligned} \tag{40}$$

$$\begin{aligned} D^{(n+1)}{}^{ia}_{jb} = &\sum_{k}\left(-D^{(n)}{}^{ka}_{jb} S^{i}_{k} + D^{(n)}{}^{ia}_{kb} S^{k}_{j} - D^{(n)}{}^{k}_{b} S^{ia}_{jk}\right) \\ &+ \frac{1}{2}\sum_{kl} D^{(n)}{}^{kl}_{jb} S^{ia}_{kl} + \sum_{ck} D^{(n)}{}^{ka}_{cb} S^{ic}_{jk}, \end{aligned} \tag{41}$$

$$D^{(n+1)}{}^{ab}_{cd} = 0, \tag{42}$$

and

$$\begin{aligned} D^{(n+1)}{}^{ij}_{kl} = &\frac{1}{2}\sum_{mn}\left(D^{(n)}{}^{mn}_{kl} S^{ij}_{mn} - S^{mn}_{kl} D^{(n)}{}^{ij}_{mn}\right) \\ &+ \sum_{m}(1-P_{ij})\left(-D^{(n)}{}^{im}_{kl} S^{j}_{m} + S^{im}_{kl} D^{(n)}{}^{j}_{m}\right) \\ &+ \sum_{m}(1-P_{kl})\left(D^{(n)}{}^{ij}_{km} S^{m}_{l} - S^{ij}_{km} D^{m}_{l}\right) \\ &+ \sum_{a}(1-P_{ij}) D^{(n)}{}^{j}_{a} S^{ia}_{kl} \\ &+ \sum_{am}(1-P_{ij})(1-P_{kl}) D^{(n)}{}^{im}_{ka} S^{ja}_{lm}, \end{aligned} \tag{43}$$

$$D^{(n+1)}{}^{ab}_{ic} = \sum_{k} D^{(n)}{}^{ab}_{kc} S^{k}_{i}, \tag{44}$$

$$\begin{aligned} D^{(n+1)}{}^{ia}_{jk} = &\frac{1}{2}\sum_{mn}\left(D^{(n)}{}^{mn}_{jk} S^{ia}_{mn} - S^{mn}_{jk} D^{(n)}{}^{ia}_{mn}\right) \\ &+ \sum_{l}\left(-D^{(n)}{}^{la}_{jk} S^{i}_{l} + S^{la}_{jk} D^{(n)}{}^{i}_{l}\right) \\ &+ \sum_{l}(1-P_{jk})\left(D^{(n)}{}^{ia}_{lk} S^{l}_{j} - S^{ia}_{lk} D^{(n)}{}^{l}_{j}\right) \\ &+ \sum_{b} D^{(n)}{}^{a}_{b} S^{ib}_{jk} \\ &- \sum_{cl}(1-P_{jk}) D^{(n)}{}^{la}_{kc} S^{ic}_{jl}, \end{aligned} \tag{45}$$

$$D^{(n+1)}{}^{ij}_{ab} = \frac{1}{2}\sum_{kl} D^{(n)}{}^{kl}_{ab} S^{ij}_{kl} - \sum_{k}(1-P_{ij}) D^{(n)}{}^{ik}_{ab} S^{j}_{k}. \tag{46}$$

Equations (31) and (42) imply that the hole-hole interaction is not affected by a particle-particle decoupling, meanwhile the particle-particle interaction is not changed by a hole-hole decoupling. This is true only in a single commutator, and the interplay between the *hh* and *pp* decoupling occurs in the nested commutator. This suggests that the *pp* interaction is weakly affected by the *hh* decoupling, because of the diminishing importance of increasingly nested commutators. In practical calculations, the effective *pp* interaction from a particle-hole decoupling is not identical to that from a *pp* decoupling, but as expected they do reproduce the same eigenvalues.

In the particle-hole decoupling, valence particles and holes need to be treated on an equal footing. The possibility of particle-hole de-excitation in the valence space complicates the decoupling, as each sector of the Hamiltonian need to be decoupled, see Fig. 3. In most shell-model calculations, we do not usually need protons or neutrons to be particle and hole states simultaneously. In the current work, we restrict ourselves to a model space that contains only neutron particles and proton hole states (or verse vice). The off-diagonal Hamiltonian contains no particle-hole de-excitations due to isospin conservation, and only the last term in Fig. 3 contributes. The S operator for the particle-hole decoupling is

$$S = S_{hh} + S_{pp} + S_{hp}. \tag{47}$$

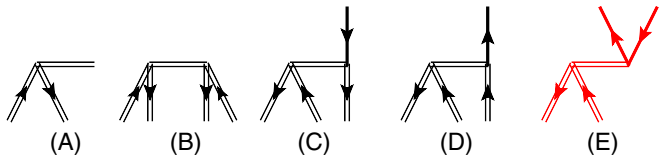

FIG. 3. Diagrammatic representation of S_{hp}. The horizontal line is the S_{hp} operator, with the particles indicated by incoming and outgoing arrow lines. The valence space particles and holes are indicated by incoming double lines. (A) represents a particle-hole de-excitation in the valence space, (B) a valence space $2p$–$2h$ de-excitation, (C) a valence-space $2h$–$1p$ coupled to one hole, (D) a valence-space $2p$–$1h$ coupled to one particle, and (E) represent valence-space particle-hole coupled to a particle-hole in the excluded space.

Here, S_{pp} and S_{hh} have already been discussed above and we will focus on the additional terms. Diagram E in Fig. 3 is

$$S_{hp} = \sum_{iajv} s^{v_1 a}_{jv_2} \{v_1^\dagger a^\dagger j v_2\}. \tag{48}$$

Here, S_{hp} couples the particle-hole states between the model space and the excluded space.

Additional terms contributing to the single commutator $[D^{(n)}, S_{hp}]$ are

$$D^{(n+1)}{}^{ia}_{bc} = \sum_{kd}(1-P_{bc})\left(D^{(n)}{}^{ka}_{cd} S^{id}_{kb} - S^{ka}_{cd} D^{(n)}{}^{id}_{kb}\right) - \sum_{j}(1-P_{bc}) D^{(n)}{}^{j}_{b} S^{ia}_{jc}, \tag{49}$$

$$D^{(n+1)}{}^{ij}_{ka} = \sum_{dl}(1-P_{ij})\left(-D^{(n)}{}^{il}_{kd} S^{jd}_{la} + S^{il}_{kd} D^{(n)}{}^{jd}_{la}\right) + \sum_{b}(1-P_{ij}) D^{(n)}{}^{j}_{b} S^{ib}_{ka}, \tag{50}$$

$$D^{(n+1)}{}^{ia}_{jb} = \sum_{kc}\left(-D^{(n)}{}^{ka}_{jc} S^{ic}_{kb} + S^{ka}_{jc} D^{(n)}{}^{ic}_{kb}\right) + \sum_{c}\left(D^{(n)}{}^{a}_{c} S^{ic}_{jb} - D^{(n)}{}^{c}_{b} S^{ia}_{jc}\right) + \sum_{k}\left(-D^{(n)}{}^{k}_{j} S^{ia}_{kb} + D^{(n)}{}^{i}_{k} S^{ka}_{jb}\right), \tag{51}$$

$$D^{(n+1)}{}^{ij}_{ab} = -\sum_{kc}(1-P_{ij})(1-P_{ab}) D^{(n)}{}^{ik}_{ac} S^{jc}_{kb}. \tag{52}$$

Once decoupled, the effective interaction consists of three sectors. The first sector is the typical pp interaction, for which the low-lying excited states of particles attached to the core can be calculated. The second sector is the hole-hole interaction, which can be used in hole-hole shell model calculations for particle removed systems. Another sector is the particle-hole channel, which can be used to calculate nuclei with protons removed and neutrons attached depending on the model space selected.

For a hole-hole shell-model calculation, one can use standard shell-model codes. The expectation values of the one-body interaction are calculated via

$$\langle ij|f_{pq}\{p^\dagger q\}|kl\rangle = -f_{ki}\delta_{jl} - f_{lj}\delta_{ik} + f_{li}\delta_{jk} + f_{kj}\delta_{il}, \tag{53}$$

and two-body expectation values are

$$\langle ij|f_{pqrs}\{p^\dagger q^\dagger rs\}|kl\rangle = f_{klij}. \tag{54}$$

The particle-hole interaction is more complicated. The one-body operator is applied as

$$\langle ai^{-1}|f_{pq}\{p^\dagger q\}|bj^{-1}\rangle = f_{ab}\delta_{ij} - f_{ji}\delta_{ab}. \tag{55}$$

The two-body operator needs an explicit Pandya transformation [70]

$$\langle ai^{-1}|V|bj^{-1}\rangle^J = -\sum_{J'} J'^2 \begin{Bmatrix} j_a & j_i & J \\ j_b & j_j & J' \end{Bmatrix} \langle aj|V|bi\rangle^{J'}. \tag{56}$$

The interaction can also be re-normal-ordered with respect to a lighter core where all single-particle orbitals are particle states. The shell-model effective interaction from SMCC is non-Hermitian. To be used in standard shell model codes, the effective interaction can be made Hermitian [49] through

$$H^{\rm hm}_{\rm eff} = [\omega^\dagger\omega]^{1/2} H^{\rm nhm}_{\rm eff} [\omega^\dagger\omega]^{-1/2}. \tag{57}$$

Here, ω is the matrix that diagonalizes the non-Hermitian Hamiltonian $H^{\rm nhm}_{\rm eff}$. The Hermitian $H^{\rm hm}_{\rm eff}$ contains one and two-body terms and can be used in conventional shell-model calculations.

The truncation at the two-body level is a reasonable first approximation in SMCC and VS-IMSRG. However, The off-diagonal three-body force $S^{\rm od}_{3b}$ induced by the similarity transformation cannot be neglected for an accurate description of nuclei. The full three-body decoupling is computationally very expensive and challenging to implement. However, the leading contribution from $S^{\rm od}_{3b}$ is accessible through a linearized approximation in the BCH expansion (22) and captures the important parts of three-body correlations [26]. We discuss this correction next.

The leading contributions from induced three-body terms comes from Eq. (26), and that approximation neglects induced three-body terms from any of the nested commutators. The operator $\overline{\overline{\mathcal{H}}}_{3b}$ can be split into diagonal $\overline{\overline{\mathcal{H}}}^{\rm da}_{3b}$ and off-diagonal $\overline{\overline{\mathcal{H}}}^{\rm od}_{3b}$ contributions. Suppose $\overline{\overline{\mathcal{H}}}^{\rm od}_{3b}$ is driven to zero in a third similarity transformation

$$Qe^{-S_{3b}}\overline{\overline{\mathcal{H}}}e^{S_{3b}}P = 0, \tag{58}$$

where S_{3b} couples the valence space and excluded space at the three-body level. This operator would feed back to the two-body decoupling equation, breaking the two-body level decoupling condition $Q\overline{\overline{\mathcal{H}}}P = 0$. As an approximation, we assume this feedback can be neglected, because in a proper decoupling, the induced $\overline{\overline{\mathcal{H}}}_{3b}$ should be small compared to $\overline{\overline{\mathcal{H}}}_{2b}$. The left-hand side of Eq. (58) can therefore be written as

$$Qe^{-S_{3b}}\overline{\overline{\mathcal{H}}}e^{S_{3b}}P \approx Q(1-S_{3b})\overline{\overline{\mathcal{H}}}(1+S_{3b})P \tag{59}$$

$$\approx Q\overline{\overline{\mathcal{H}}}P + Q[\overline{\overline{\mathcal{H}}}, S_{3b}]P. \tag{60}$$

Substitution of Eq. (60) into Eq. (58) yields the decoupling equation that determines S_{3b}; these are

$$Q\overline{\overline{\mathcal{H}}}_{1b}P + Q[\overline{\overline{\mathcal{H}}}, S_{3b}]_{1b}P \approx 0, \tag{61}$$

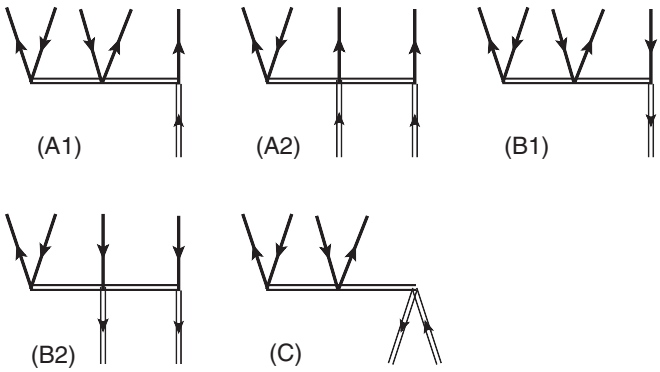

FIG. 4. Diagrammatic representation of S_{3b}. The horizontal line is the S_{3b} operator, with the particles indicated by incoming and outgoing arrow lines. The model-space particles and holes are indicated by incoming and outgoing double lines respectively. A1 and A2 are used in particle-particle decoupling, B1 and B2 for hole-hole decoupling, and all A, B, and C diagrams are used for particle-hole decoupling.

$$Q\overline{\overline{\mathcal{H}}}_{2b}P + Q[\overline{\overline{\mathcal{H}}}, S_{3b}]_{2b}P \approx 0, \tag{62}$$

$$Q\overline{\overline{\mathcal{H}}}_{3b}P + Q[\overline{\overline{\mathcal{H}}}, S_{3b}]_{3b}P \approx 0. \tag{63}$$

As we have assumed that $Q\overline{\overline{\mathcal{H}}}P = 0$ is preserved on the two-body level, Eqs. (61) and (62) are trivial, whereas S_{3b} can be determined by Eq. (63). If we keep only the diagonal one-body part in $\overline{\overline{\mathcal{H}}}$, the operator S_{3b} has the simple form

$$\langle pqu|S_{3b}|rst\rangle = \frac{\langle pqu|\overline{\overline{\mathcal{H}}}_{3b}|rst\rangle}{\overline{\overline{\mathcal{H}}}_{pp} + \overline{\overline{\mathcal{H}}}_{qq} + \overline{\overline{\mathcal{H}}}_{uu} - \overline{\overline{\mathcal{H}}}_{rr} - \overline{\overline{\mathcal{H}}}_{ss} - \overline{\overline{\mathcal{H}}}_{tt}}. \tag{64}$$

Figure 4 shows the diagrams included in S_{3b}. The diagrams A1 and A2 couple the valence particles to the excluded space. Diagrams B1 and B2 couple the valence holes and the excluded space, and diagram C couples the particle-hole states to the excluded space in the isospin $T_z = \pm 1$ channels.

With S_{3b}, the effective shell model interaction becomes

$$H_{1b}^{\text{eff}} = P\overline{\overline{\mathcal{H}}}_{1b}P + P[\overline{\overline{\mathcal{H}}}, S_{3b}]_{1b}P, \tag{65}$$

$$H_{2b}^{\text{eff}} = P\overline{\overline{\mathcal{H}}}_{2b}P + P[\overline{\overline{\mathcal{H}}}, S_{3b}]_{2b}P. \tag{66}$$

The final effective interaction is thereby decoupled at the two-body level and three-body corrections are included in a linearized approximation.

III. RESULTS

We use two chiral interactions to compute the corresponding shell-model effective interactions. The first is the 1.8/2.0(EM) potential [71] which results from a similarity-renormalization-group (SRG) transformation [72] at cutoff $\lambda = 1.8$ fm^{-1} of the N^{3}LO(EM) nucleon-nucleon potential from [73], and the three-body potential is given at N^{2}LO in chiral EFT [74–76] with a cutoff $\Lambda_{NNN} = 2.0$ fm^{-1}. The second potential is the ΔNNLO$_{\text{GO}}$ with a cutoff $\Lambda = 394$ MeV [77]. This nucleon-nucleon and three-nucleon interaction includes Δ degrees of freedom. With both interactions we perform a Hartree-Fock (HF) calculation in the harmonic oscillator basis with a frequency of $\hbar\omega = 16$ MeV. The model space is spanned by 13 shells ($N_{\max} = 12$), and the three-body matrix elements are truncated at $E_{3\max} = 16\hbar\omega$. The two-body and three-body interaction is then normal ordered with respect to the ^{100}Sn core. The CC calculations are performed with the normal-ordered two-body interaction.

TABLE I. Single-particle energies calculated with the 1.8/2.0(EM) and ΔNNLO$_{\text{GO}}$ potentials. $p_{3/2}$, $p_{1/2}$, and $g_{9/2}$ are hole states with respect to ^{100}Sn, and the remaining states are particle states.

s.p. energy (MeV)		1.8/2.0(EM)	ΔNNLO$_{\text{GO}}$
holes	$p_{3/2}$	−6.502	−4.798
	$p_{1/2}$	−4.871	−3.159
	$g_{9/2}$	−3.106	−2.267
particles	$g_{7/2}$	−10.832	−10.072
	$d_{5/2}$	−10.548	−9.375
	$d_{3/2}$	−8.054	−6.811
	$s_{1/2}$	−7.789	−6.220
	$h_{11/2}$	−5.596	−5.012

We use ^{100}Sn as the core, with the model space spanned by neutron-particle and proton-hole states. Using the effective shell-model interactions, we studied the nuclei southeast of ^{100}Sn by removing protons and attaching neutrons. To decouple the core, we employed the CCSDT-1 approximation [78] for both potentials. Using the highly optimized nuclear tensor contraction library (NTCL) [79] we are able to perform these calculations in the full space (without truncating the number of triples amplitudes) on SUMMIT, the supercomputer of the U.S. Department of Energy with a peak performance of 200 petaflops which is operated by the Oak Ridge Leadership Computing Facility at Oak Ridge National Laboratory.

The resulting binding energy of ^{100}Sn is −837 MeV and −816 MeV for 1.8/2.0(EM) and ΔNNLO$_{\text{GO}}$, respectively, compared to the datum of −825.3 MeV. The proton model space includes the $p_{3/2}$, $p_{1/2}$, and $g_{9/2}$ orbitals, and the neutron space consists of $g_{7/2}$, $d_{5/2}$, $d_{3/2}$, $s_{1/2}$, and $h_{11/2}$. We decouple the Hamiltonian at the two-body level, and include the off-diagonal three-body terms approximately according to Eqs. (65) and (66).

Table I shows the calculated single-particle and single-hole energies from the two chiral potentials. For ^{101}Sn, the experimental splitting is a 171 keV between the $5/2^+$ and the $7/2^+$ states [35,36]. In our calculation the 1.8/2.0(EM) yields the $E(g_{7/2})$ 284 keV lower than $E(d_{5/2})$, which agrees with the PA-EOM-CC and VS-IM-SRG calculations [46]. Meanwhile, the splitting from ΔNNLO$_{\text{GO}}$ is 700 keV, which is a bit larger than the datum. Both potentials predict a $9/2^+$ ground state of ^{99}In, which has a single-hole configuration. Matrix elements of these interactions are available in the Supplemental Material [80].

Figure 5 shows the calculated binding energies of two-particle (^{102}Sn), two-hole (^{98}Cd), and one-particle–one-hole

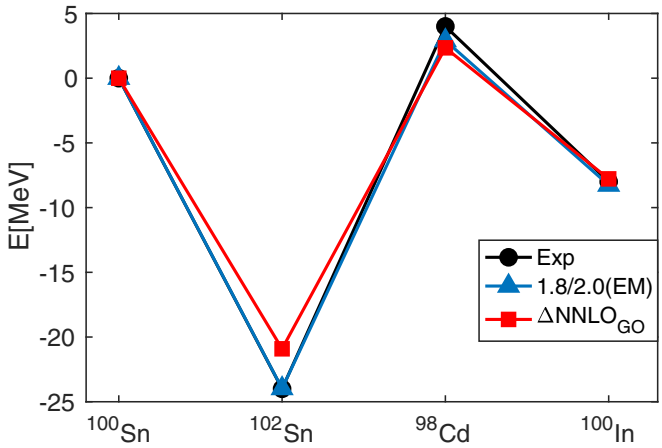

FIG. 5. Ground-state energies of ^{102}Sn, ^{98}Cd, and ^{100}In relative to ^{100}Sn, calculated with 1.8/2.0(EM) and ΔNNLO$_{GO}$ potential and compared to experimental data. We used an arbitrary energy shift of 90 keV between the (6^+) and (5^+) levels.

(^{100}In) nuclei with respect to the ground state of ^{100}Sn. The 1.8/2.0(EM) potential is in agreement with the experimental data. The ΔNNLO$_{GO}$ somewhat underestimates ^{102}Sn and overbinds the two-proton system ^{98}Cd. The two potentials coincide in ^{100}In. In a simple non-interacting shell-model picture, the ground state of ^{100}In depends on $E(\pi g_{7/2}) - E(\nu g_{9/2})$, and the coincidence in ^{100}In is indicated from our calculated single-particle energies.

The spectra of the two-hole state nucleus ^{98}Cd and the particle-hole nucleus ^{100}In are shown in Fig. 6. For cadmium, the 1.8/2.0(EM) interaction yields an accurate spectrum while the ΔNNLO$_{GO}$ potential yields a spectrum that is too compressed. The dominant configuration for ^{98}Cd is two holes in $\pi g_{9/2}$. The ΔNNLO$_{GO}$ generates a small matrix element $\langle \pi g_{9/2} \pi g_{9/2} | V | \pi g_{9/2} \pi g_{9/2} \rangle^J$, and this leads to the compressed spectrum. The odd-odd nucleus ^{100}In has a high level density close to the ground state with quasidegenerate $J^\pi = 2^+ \cdots 7^+$ states, stemming from the coupling of a $\pi g_{9/2}$ hole to the almost degenerate $\nu g_{7/2}$ and $\nu d_{5/2}$ particle states. While the experimental spectrum is unknown [37] regarding spin assignments and the energy shift with respect to the

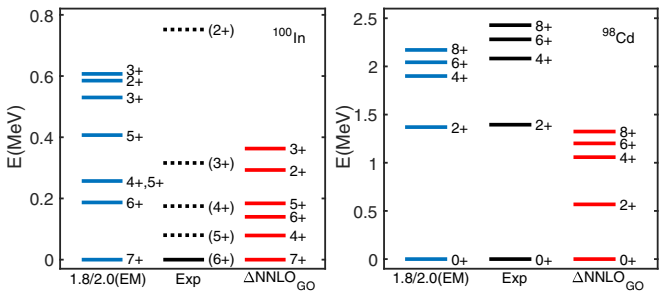

FIG. 6. Low-energy spectra of ^{98}Cd (right) and ^{100}In (left) calculated with 1.8/2.0(EM) and ΔNNLO$_{GO}$ potentials, respectively, and compared to experimental data. For ^{100}In, the energies of the experimentally known excited states (shown as dotted lines) have an unknown shift with respect to the ground state [37].

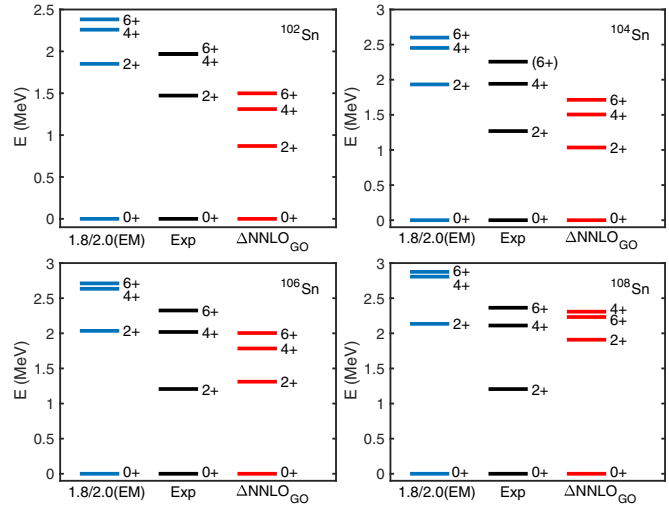

FIG. 7. Calculated low-lying excited states in Sn isotopes with the 1.8/2.0(EM) (blue) and ΔNNLO$_{GO}$ (red) potentials, and compared to data (black).

ground state, the level density from the 1.8/2.0(EM) interaction is more accurate than that from the ΔNNLO$_{GO}$ potential. We also note that the level density of the 1.8/2.0(EM) interaction agrees with the coupled-cluster results shown in Fig. 4 of the Supplementary Information of Ref. [38]. The ground-state spin of ^{100}In is not known experimentally [81], and both interactions yield a 7^+ ground state. However, our estimated uncertainties of about 0.2 MeV are too large to make a prediction here.

The tin isotopes depend only on the neutron-neutron interaction, i.e., the particle-particle interaction constructed in this work. Figure 7 shows the low-lying excited states calculated for $^{102-104}$Sn. The 1.8/2.0(EM) potential yields a near constant 2^+ energy, in agreement with the VS-IMSRG calculation of Ref. [46]. The ΔNNLO$_{GO}$ potential also gives a near constant $E(2^+)$ energy (with the exception of ^{108}Sn), but generally lower in excitation energy than obtained using the 1.8/2.0(EM) potential. Data fall in-between the two employed potentials for ^{102,104}Sn, for ^{106}Sn the results obtained with ΔNNLO$_{GO}$ agrees well with data, while for ^{108}Sn both potentials overestimate the $E(2^+)$ energy. The difference in the $E(2^+)$ energies obtained from the two potentials stems mostly from the associated single-particle energies given in Table I.

The cadmium isotopes are obtained by removing two protons from ^{100}Sn core and adding neutrons. Our calculations, shown in Fig. 8, indicate that the removed neutrons are mainly from $g_{9/2}$ and the spectra of cadmium isotopes are mostly determined by the neutron configurations. Similar to the tin isotopes, the 2^+ states for even-even cadmium from 1.8/2.0(EM) are higher than the data, and the ΔNNLO$_{GO}$ shows a slight increase of $E(2^+)$ as the neutron number increases.

The two potentials produce more differences in the indium isotopes, which remove one proton and add neutrons to the ^{100}Sn core. The odd-mass indium nuclei, shown in Fig. 9, have $9/2^+$ ground states and a first $1/2^-$ low-lying excited state (with the exception of ^{101}In) according to the experimental

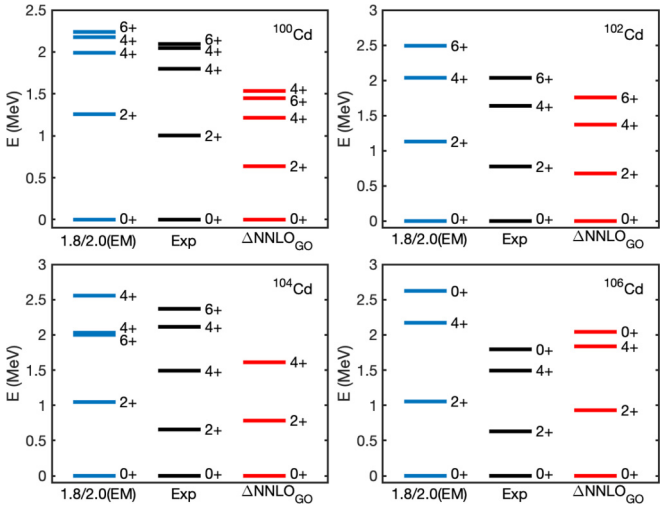

FIG. 8. Calculated low-lying excited states in Cd isotopes with the 1.8/2.0(EM) (blue) and ΔNNLO$_{\rm GO}$ (red) potentials, and compared to data (black).

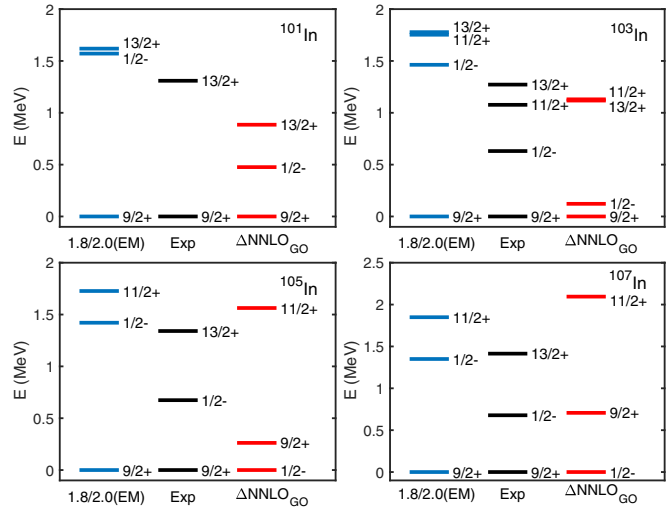

FIG. 9. Calculated low-lying excited states in In isotopes with the 1.8/2.0(EM) (blue) and ΔNNLO$_{\rm GO}$ (red) potentials, and compared to data (black).

data. The 1.8/2.0(EM) potential reproduces the correct order of the ground states and the $1/2^-$ excited state in $^{101-107}$In. The computed $1/2^-$ state is generally higher than the data, which may be due to a too large gap between the $g_{9/2}$ and $p_{1/2}$ orbitals. The ΔNNLO$_{\rm GO}$ reproduces the correct level ordering in ^{101,103}In, but fails to reproduce the correct ground state of ^{105,107}In. In contrast to tin and cadmium isotopes, the indium isotopes exhibit more proton and neutron correlations. Finally, we note that uncertainties stemming from model-space truncations and the approximate treatment of normal-ordered three-body forces away from the ^{100}Sn core will impact the results. In the recent work [44] we estimated that empirical pairing gaps in this mass region computed with the SMCC and employing the same Hamiltonians carried an uncertainty of about $\pm$0.2 MeV.

IV. SUMMARY

We presented a systematic derivation of the particle-hole variant of the shell-model coupled-cluster method to compute nuclei in the vicinity of ^{100}Sn. The shell-model effective interaction is defined in a model space consisting of both particles and holes. The decoupling of the model space from the excluded space is accomplished at the two-body level, and the induced off-diagonal three-body terms are included in a linearized approximation. For nuclei in the vicinity of ^{100}Sn the particle-hole effective interaction benefits from a more favorable reference state and more realistic mean-field than, e.g., taking a ^{88}Sr core. The computational resources required for nuclei close to the core are also reduced by introducing explicit hole states in the shell model. The method is validated through cross-benchmark with the existing *ab-initio* methods. We derived effective interactions from two sets of chiral potentials that include nucleon-nucleon and three-nucleon forces, and computed properties of tin, indium, and cadmium isotopes. Binding energies and spectra exhibit a good to fair agreement with data.

ACKNOWLEDGMENTS

This material is based upon work supported by the U.S. Department of Energy, Office of Science, Office of Nuclear Physics under Awards No. DEFG02-96ER40963 (University of Tennessee), No. DE-SC0008499 (SciDAC-3 NUCLEI), No. DE-SC0018223 (SciDAC-4 NUCLEI), No. DE-SC0015376 (Double-Beta Decay Topical Collaboration), and the Field Work Proposals ERKBP57 and ERKBP72 at Oak Ridge National Laboratory (ORNL). Computer time was provided by the Innovative and Novel Computational Impact on Theory and Experiment (INCITE) program. This research used resources of the Oak Ridge Leadership Computing Facility located at ORNL, which is supported by the Office of Science of the Department of Energy under Contract No. DE-AC05-00OR22725.

[1] M. G. Mayer and J. H. D. Jensen, *Elementary Theory of Nuclear Shell Structure* (John Wiley & Sons, New York, 1955).

[2] B. A. Brown and B. H. Wildenthal, Status of the nuclear shell model, Annu. Rev. Nucl. Part. Sci. **38**, 29 (1988).

[3] T. Otsuka, M. Honma, T. Mizusaki, N. Shimizu, and Y. Utsuno, Monte Carlo shell model for atomic nuclei, Prog. Part. Nucl. Phys. **47**, 319 (2001).

[4] E. Caurier, G. Martínez-Pinedo, F. Nowacki, A. Poves, and A. P. Zuker, The shell model as a unified view of nuclear structure, Rev. Mod. Phys. **77**, 427 (2005).

[5] S. R. Stroberg, H. Hergert, S. K. Bogner, and J. D. Holt, Nonempirical interactions for the nuclear shell model: An update, Annu. Rev. Nucl. Part. Sci. **69**, 307 (2019).

[6] B. A. Brown, The nuclear shell model towards the drip lines, Prog. Part. Nucl. Phys. **47**, 517 (2001).

[7] B. A. Brown and W. A. Richter, New "usd" Hamiltonians for the sd shell, Phys. Rev. C **74**, 034315 (2006).

[8] M. Honma, T. Otsuka, B. A. Brown, and T. Mizusaki, New effective interaction for pf-shell nuclei and its implications for the stability of the $n = z = 28$ closed core, Phys. Rev. C **69**, 034335 (2004).

[9] A. Poves and A. Zuker, Theoretical spectroscopy and the fp shell, Phys. Rep. **70**, 235 (1981).

[10] M. Hjorth-Jensen, T. T. S. Kuo, and E. Osnes, Realistic effective interactions for nuclear systems, Phys. Rep. **261**, 125 (1995).

[11] T. T. S. Kuo and G. E. Brown, Reaction matrix elements for the 0f-1p shell nuclei, Nucl. Phys. A **114**, 241 (1968).

[12] T. T. S. Kuo, S. Y. Lee, and K. F. Ratcliff, A folded-diagram expansion of the model-space effective Hamiltonian, Nucl. Phys. A **176**, 65 (1971).

[13] B. R. Barrett and M. W. Kirson, Higher-order terms and the apparent non-convergence of the perturbation expansion for the effective interaction in finite nuclei, Nucl. Phys. A **148**, 145 (1970).

[14] T. H. Schucan and H. A. Weidenmüller, Perturbation theory for the effective interaction in nuclei, Ann. Phys. (NY) **76**, 483 (1973).

[15] E. M. Krenciglowa and T. T. S. Kuo, Convergence of effective Hamiltonian expansion and partial summations of folded diagrams, Nucl. Phys. A **235**, 171 (1974).

[16] R. Okamoto, K. Suzuki, H. Kumagai, and S. Fujii, A new solution for effective interaction, J. Phys.: Conf. Ser. **267**, 012017 (2011).

[17] L. Coraggio, A. Covello, A. Gargano, N. Itaco, and T. T. S. Kuo, Effective shell-model Hamiltonians from realistic nucleon-nucleon potentials within a perturbative approach, Ann. Phys. (NY) **327**, 2125 (2012).

[18] S. K. Bogner, T. T. S. Kuo, and A. Schwenk, Model-independent low momentum nucleon interaction from phase shift equivalence, Phys. Rep. **386**, 1 (2003).

[19] L. Coraggio, A. Covello, A. Gargano, N. Itaco, and T. T. S. Kuo, Shell-model calculations and realistic effective interactions, Prog. Part. Nucl. Phys. **62**, 135 (2009).

[20] L. Coraggio, A. Covello, A. Gargano, and N. Itaco, Realistic shell-model calculations for neutron-rich calcium isotopes, J. Phys.: Conf. Ser. **267**, 012021 (2011).

[21] S. K. Bogner, H. Hergert, J. D. Holt, A. Schwenk, S. Binder, A. Calci, J. Langhammer, and R. Roth, Nonperturbative Shell-Model Interactions from the in-Medium Similarity Renormalization Group, Phys. Rev. Lett. **113**, 142501 (2014).

[22] G. R. Jansen, J. Engel, G. Hagen, P. Navratil, and A. Signoracci, *Ab Initio* Coupled-Cluster Effective Interactions for the Shell Model: Application to Neutron-Rich Oxygen and Carbon Isotopes, Phys. Rev. Lett. **113**, 142502 (2014).

[23] G. R. Jansen, M. D. Schuster, A. Signoracci, G. Hagen, and P. Navrátil, Open sd-shell nuclei from first principles, Phys. Rev. C **94**, 011301(R) (2016).

[24] S. R. Stroberg, H. Hergert, J. D. Holt, S. K. Bogner, and A. Schwenk, Ground and excited states of doubly open-shell nuclei from *ab initio* valence-space Hamiltonians, Phys. Rev. C **93**, 051301(R) (2016).

[25] E. Dikmen, A. F. Lisetskiy, B. R. Barrett, P. Maris, A. M. Shirokov, and J. P. Vary, *Ab initio* effective interactions for sd-shell valence nucleons, Phys. Rev. C **91**, 064301 (2015).

[26] Z. H. Sun, T. D. Morris, G. Hagen, G. R. Jansen, and T. Papenbrock, Shell-model coupled-cluster method for open-shell nuclei, Phys. Rev. C **98**, 054320 (2018).

[27] T. Miyagi, T. Abe, M. Kohno, P. Navrátil, R. Okamoto, T. Otsuka, N. Shimizu, and S. R. Stroberg, Ground-state properties of doubly magic nuclei from the unitary-model-operator approach with chiral two- and three-nucleon forces, Phys. Rev. C **100**, 034310 (2019).

[28] K. Suzuki and S. Y. Lee, Convergent theory for effective interaction in nuclei, Prog. Theor. Phys. **64**, 2091 (1980).

[29] K. Suzuki, Construction of hermitian effective interaction in nuclei: general relation between hermitian and non-Hermitian forms, Prog. Theor. Phys. **68**, 246 (1982).

[30] H. Kümmel, K. H. Lührmann, and J. G. Zabolitzky, Many-fermion theory in expS- (or coupled cluster) form, Phys. Rep. **36**, 1 (1978).

[31] G. Hagen, T. Papenbrock, M. Hjorth-Jensen, and D. J. Dean, Coupled-cluster computations of atomic nuclei, Rep. Prog. Phys. **77**, 096302 (2014).

[32] K. Tsukiyama, S. K. Bogner, and A. Schwenk, In-Medium Similarity Renormalization Group for Nuclei, Phys. Rev. Lett. **106**, 222502 (2011).

[33] K. Tsukiyama, S. K. Bogner, and A. Schwenk, In-medium similarity renormalization group for open-shell nuclei, Phys. Rev. C **85**, 061304(R) (2012).

[34] H. Hergert, S. K. Bogner, T. D. Morris, A. Schwenk, and K. Tsukiyama, The in-medium similarity renormalization group: A novel ab initio method for nuclei, Phys. Rep. **621**, 165 (2016).

[35] D. Seweryniak, K. Starosta, C. N. Davids, S. Gros, A. A. Hecht, N. Hoteling, T. L. Khoo, K. Lagergren, G. Lotay, D. Peterson, A. Robinson, C. Vaman, W. B. Walters, P. J. Woods, and S. Zhu, α decay of ^{105}Te, Phys. Rev. C **73**, 061301(R) (2006).

[36] I. G. Darby, R. K. Grzywacz, J. C. Batchelder, C. R. Bingham, L. Cartegni, C. J. Gross, M. Hjorth-Jensen, D. T. Joss, S. N. Liddick, W. Nazarewicz, S. Padgett, R. D. Page, T. Papenbrock, M. M. Rajabali, J. Rotureau, and K. P. Rykaczewski, Orbital Dependent Nucleonic Pairing in the Lightest Known Isotopes of Tin, Phys. Rev. Lett. **105**, 162502 (2010).

[37] C. B. Hinke, M. Böhmer, P. Boutachkov, T. Faestermann, H. Geissel, J. Gerl, R. Gernhäuser, M. Gorska, A. Gottardo, H. Grawe, J. L. Grebosz, R. Krücken, N. Kurz, Z. Liu, L. Maier, F. Nowacki, S. Pietri, Zs. Podolyák, K. Sieja, K. Steiger *et al.*, Superallowed Gamow-Teller decay of the doubly magic nucleus ^{100}Sn, Nature (London) **486**, 341 (2012).

[38] P. Gysbers, G. Hagen, J. D. Holt, G. R. Jansen, T. D. Morris, P. Navrátil, T. Papenbrock, S. Quaglioni, A. Schwenk, S. R. Stroberg, and K. A. Wendt, Discrepancy between experimental and theoretical β-decay rates resolved from first principles, Nat. Phys. **15**, 428 (2019).

[39] D. Lubos, J. Park, T. Faestermann, R. Gernhäuser, R. Krücken, M. Lewitowicz, S. Nishimura, H. Sakurai, D. S. Ahn, H. Baba, B. Blank, A. Blazhev, P. Boutachkov, F. Browne, I. Čeliković, G. de France, P. Doornenbal, Y. Fang, N. Fukuda, J. Giovinazzo *et al.*, Improved Value for the Gamow-Teller Strength of the ^{100}Sn Beta Decay, Phys. Rev. Lett. **122**, 222502 (2019).

[40] F. Herfurth, G. Audi, D. Beck, K. Blaum, G. Bollen, P. Delahaye, M. Dworschak, S. George, C. Guénaut, A. Kellerbauer, D. Lunney, M. Mukherjee, S. Rahaman, S. Schwarz, L. Schweikhard, C. Weber, and C. Yazidjian, New mass data for the rp-process above $Z = 32$, Eur. Phys. J. A **47**, 75 (2011).

[41] R. Ferrer, N. Bree, T. E. Cocolios, I. G. Darby, H. De Witte, W. Dexters, J. Diriken, J. Elseviers, S. Franchoo, M. Huyse, N. Kesteloot, Yu. Kudryavtsev, D. Pauwels, D. Radulov, T. Roger, H. Savajols, P. Van Duppen, and M. Venhart, In-gas-cell laser ionization spectroscopy in the vicinity of ^{100}Sn: Magnetic moments and mean-square charge radii of $N = 50 - 54$ Ag, Phys. Lett. B **728**, 191 (2014).

[42] X. Xu, J. H. Liu, C. X. Yuan, Y. M. Xing, M. Wang, Y. H. Zhang, X. H. Zhou, Yu. A. Litvinov, K. Blaum, R. J. Chen, X. C. Chen, C. Y. Fu, B. S. Gao, J. J. He, S. Kubono, Y. H. Lam, H. F. Li, M. L. Liu, X. W. Ma, P. Shuai *et al.*, Masses of ground and isomeric states of ^{101}In and configuration-dependent shell evolution in odd-*a* indium isotopes, Phys. Rev. C **100**, 051303(R) (2019).

[43] C. Hornung, D. Amanbayev, I. Dedes, G. Kripko-Koncz, I. Miskun, N. Shimizu, S. Ayet San Andrés, J. Bergmann, T. Dickel, J. Dudek, J. Ebert, H. Geissel, M. Górska, H. Grawe, F. Greiner, E. Haettner, T. Otsuka, W. R. Plaß, S. Purushothaman, A.-K. Rink *et al.*, Isomer studies in the vicinity of the doubly-magic nucleus ^{100}Sn: Observation of a new low-lying isomeric state in ^{97}Ag, Phys. Lett. B **802**, 135200 (2020).

[44] M. Mougeot, D. Atanasov, J. Karthein, R. N. Wolf, P. Ascher, K. Blaum, K. Chrysalidis, G. Hagen, J. D. Holt, W. J. Huang, G. R. Jansen, I. Kulikov, Yu. A. Litvinov, D. Lunney, V. Manea, T. Miyagi, T. Papenbrock, L. Schweikhard, A. Schwenk, T. Steinsberger *et al.*, Mass measurements of $^{99-101}$In challenge ab initio nuclear theory of the nuclide ^{100}Sn, Nat. Phys. **17**, 1099 (2021).

[45] T. Faestermann, M. Górska, and H. Grawe, The structure of ^{100}Sn and neighbouring nuclei, Prog. Part. Nucl. Phys. **69**, 85 (2013).

[46] T. D. Morris, J. Simonis, S. R. Stroberg, C. Stumpf, G. Hagen, J. D. Holt, G. R. Jansen, T. Papenbrock, R. Roth, and A. Schwenk, Structure of the Lightest Tin Isotopes, Phys. Rev. Lett. **120**, 152503 (2018).

[47] A. F. Lisetskiy, B. R. Barrett, M. K. G. Kruse, P. Navratil, I. Stetcu, and J. P. Vary, *Ab-initio* shell model with a core, Phys. Rev. C **78**, 044302 (2008).

[48] K. Suzuki and R. Okamoto, Effective interaction theory and unitary-model-operator approach to nuclear saturation problem, Prog. Theor. Phys. **92**, 1045 (1994).

[49] S. Ôkubo, Diagonalization of Hamiltonian and Tamm-Dancoff equation, Prog. Theor. Phys. **12**, 603 (1954).

[50] H. Hergert, In-medium similarity renormalization group for closed and open-shell nuclei, Phys. Scr. **92**, 023002 (2017).

[51] S. R. Stroberg, A. Calci, H. Hergert, J. D. Holt, S. K. Bogner, R. Roth, and A. Schwenk, Nucleus-Dependent Valence-Space Approach to Nuclear Structure, Phys. Rev. Lett. **118**, 032502 (2017).

[52] T. Miyagi, S. R. Stroberg, J. D. Holt, and N. Shimizu, *Ab initio* multishell valence-space Hamiltonians and the island of inversion, Phys. Rev. C **102**, 034320 (2020).

[53] F. Coester, Bound states of a many-particle system, Nucl. Phys. **7**, 421 (1958).

[54] D. J. Dean and M. Hjorth-Jensen, Coupled-cluster approach to nuclear physics, Phys. Rev. C **69**, 054320 (2004).

[55] R. J. Bartlett and M. Musiał, Coupled-cluster theory in quantum chemistry, Rev. Mod. Phys. **79**, 291 (2007).

[56] S. Binder, P. Piecuch, A. Calci, J. Langhammer, P. Navrátil, and R. Roth, Extension of coupled-cluster theory with a noniterative treatment of connected triply excited clusters to three-body Hamiltonians, Phys. Rev. C **88**, 054319 (2013).

[57] G. Hagen, M. Hjorth-Jensen, G. R. Jansen, and T. Papenbrock, Emergent properties of nuclei from ab initio coupled-cluster calculations, Phys. Scr. **91**, 063006 (2016).

[58] G. Hagen, T. Papenbrock, D. J. Dean, A. Schwenk, A. Nogga, M. Włoch, and P. Piecuch, Coupled-cluster theory for three-body Hamiltonians, Phys. Rev. C **76**, 034302 (2007).

[59] R. Roth, S. Binder, K. Vobig, A. Calci, J. Langhammer, and P. Navrátil, Medium-Mass Nuclei with Normal-Ordered Chiral $NN+3N$ Interactions, Phys. Rev. Lett. **109**, 052501 (2012).

[60] G. Hagen, G. R. Jansen, and T. Papenbrock, Structure of ^{78}Ni from First-Principles Computations, Phys. Rev. Lett. **117**, 172501 (2016).

[61] S. J. Novario, G. Hagen, G. R. Jansen, and T. Papenbrock, Charge radii of exotic neon and magnesium isotopes, Phys. Rev. C **102**, 051303(R) (2020).

[62] Y. Qiu, T. M. Henderson, J. Zhao, and G. E. Scuseria, Projected coupled cluster theory, J. Chem. Phys. **147**, 064111 (2017).

[63] H. Yuan and D. Cremer, Spin-projected coupled-cluster theory with single and double excitations, Theor. Chem. Acc. **105**, 132 (2000).

[64] G. R. Jansen, M. Hjorth-Jensen, G. Hagen, and T. Papenbrock, Toward open-shell nuclei with coupled-cluster theory, Phys. Rev. C **83**, 054306 (2011).

[65] G. R. Jansen, Spherical coupled-cluster theory for open-shell nuclei, Phys. Rev. C **88**, 024305 (2013).

[66] A. Ekström, G. R. Jansen, K. A. Wendt, G. Hagen, T. Papenbrock, B. D. Carlsson, C. Forssén, M. Hjorth-Jensen, P. Navrátil, and W. Nazarewicz, Accurate nuclear radii and binding energies from a chiral interaction, Phys. Rev. C **91**, 051301(R) (2015).

[67] W. Magnus, On the exponential solution of differential equations for a linear operator, Commun. Pure Appl. Math. **7**, 649 (1954).

[68] T. D. Morris, N. M. Parzuchowski, and S. K. Bogner, Magnus expansion and in-medium similarity renormalization group, Phys. Rev. C **92**, 034331 (2015).

[69] M. Heinz, A. Tichai, J. Hoppe, K. Hebeler, and A. Schwenk, In-medium similarity renormalization group with three-body operators, Phys. Rev. C **103**, 044318 (2021).

[70] S. P. Pandya, Nucleon-hole interaction in jj coupling, Phys. Rev. **103**, 956 (1956).

[71] K. Hebeler, S. K. Bogner, R. J. Furnstahl, A. Nogga, and A. Schwenk, Improved nuclear matter calculations from chiral low-momentum interactions, Phys. Rev. C **83**, 031301(R) (2011).

[72] S. K. Bogner, R. J. Furnstahl, and R. J. Perry, Similarity renormalization group for nucleon-nucleon interactions, Phys. Rev. C **75**, 061001(R) (2007).

[73] D. R. Entem and R. Machleidt, Accurate charge-dependent nucleon-nucleon potential at fourth order of chiral perturbation theory, Phys. Rev. C **68**, 041001(R) (2003).

[74] U. V. Kolck, Effective field theory of nuclear forces, Prog. Part. Nucl. Phys. **43**, 337 (1999).

[75] E. Epelbaum, A. Nogga, W. Glöckle, H. Kamada, U.-G. Meißner, and H. Witała, Three-nucleon forces from chiral effective field theory, Phys. Rev. C **66**, 064001 (2002).

[76] K. Hebeler, H. Krebs, E. Epelbaum, J. Golak, and R. Skibiński, Efficient calculation of chiral three-nucleon forces up to N^3LO for *ab initio* studies, Phys. Rev. C **91**, 044001 (2015).

[77] W. G. Jiang, A. Ekström, C. Forssén, G. Hagen, G. R. Jansen, and T. Papenbrock, Accurate bulk properties of nuclei from $a = 2$ to ∞ from potentials with Δ isobars, Phys. Rev. C **102**, 054301 (2020).

[78] Y. S. Lee, S. A. Kucharski, and R. J. Bartlett, A coupled cluster approach with triple excitations, J. Chem. Phys. **81**, 5906 (1984).

[79] G. R. Jansen, Nuclear tensor contraction library (ntcl), https://github.com/gustav-jansen/ntcl (2020).

[80] See Supplemental Material at http://link.aps.org/supplemental/10.1103/PhysRevC.104.064310 for effective shell-model interaction for nuclei southeast of ^{100}Sn.

[81] C. Plettner, L. Batist, J. Döring, A. Blazhev, H. Grawe, V. Belleguic, C. R. Bingham, R. Borcea, M. Gierlik, M. Górska, N. Harrington, Z. Janas, M. Karny, R. Kirchner, C. Mazzocchi, P. Munro, E. Roeckl, K. Schmidt, and R. Schwengner, β decay of ^{100}In, Phys. Rev. C **66**, 044319 (2002).